Electronic supplementary information

Halide perovskite as catalyst to simultaneously achieve efficient photocatalytic CO_2 reduction and methanol oxidation

Guang-Xing Dong,‡[a] Wen Zhang,‡[a] Yan-Fei Mu,[a] Ke Su,[a] Min Zhang*[ab] and Tong-Bu Lu[a]

[a] *MOE International Joint Laboratory of Materials Microstructure, Institute for New Energy Materials and Low Carbon Technologies, School of Materials Science and Engineering, Tianjin University of Technology, Tianjin 300384, China*

E-mail: zm2016@email.tjut.edu.cn.

[b] *Tianjin Key Laboratory of Organic Solar Cells and Photochemical Conversion, School of Chemistry and Chemical Engineering Department, Tianjin University of Technology, Tianjin 300384, China.*

‡ *These authors contributed equally to this work.*

Experimental Section

Materials: Cesium bromide (CsBr, ≥99.9%) and lead bromide ($PbBr_2$, ≥99.9%) were purchased from Xi'an Polymer Light Technology Corp. Cobalt bromide ($CoBr_2$, anhydrous, 97%), iron bromide ($FeBr_3$, anhydrous, 98%) and nichel bromide ($NiBr_2$, anhydrous, 99%) were purchased from Alfa Aesar. *N*,*N*-dimethylformamide (DMF, HPLC, ≥99.9%), hydrobromic acid (HBr, 48 wt% solution in water), methanol (HPLC, ≥99.9%), acetonitrile (Extra dry with molecular sieves, Water≤50 ppm, in resealable bottle, ≥99.9%), $^{13}CO_2$ and $^{13}CH_3OH$ were purchased from Sigma-Aldrich. All chemicals were purchased from commercial sources and used without further treatments. The pure $CsPbBr_3$ nanocrystals were prepared by conventional hot injection approach.[S1]

Synthesis of $CsPbBr_3/Cs_4PbBr_6$ (PNC) nanocomposites: 1 M $PbBr_2$ and 1 M CsBr were respectively ultrasonically dissolved in hydrobromic acid solution to prepare solutions **A** and **B**. Solution **A** (120 μL) was added into DMF (1 mL) and stirred vigorously in ice-bath to form $PbBr_2$ precursor. Then solution **B** (120 μL) was added into $PbBr_2$ precursor solution drop by drop and stirred in ice-bath for 3 h. Finally, dried $CsPbBr_3/Cs_4PbBr_6$ nanocrystals were obtained by drying at 80 ℃ in vacuum for 6 h after centrifuging 12000 rpm for 3 minutes, and the powder was stored in vacuum drier for further use.

Synthesis of $Co_{X\%}@CsPbBr_3/Cs_4PbBr_6$ ($Co_{x\%}@PNC$) nanocomposites: 0.01 M $CoBr_2$ was ultrasonically dissolved in DMF to prepare solution **C**. Solution **A** (120 μL) was added into a certain amount of DMF (**Table S1**) and stirred vigorously in ice-bath to form $PbBr_2$ precursor, then a certain amount of solution **C** (**Table S1**) was added into $PbBr_2$ precursor. After stirring 2 minutes, solution **B** (120 μL) was added into $PbBr_2$ precursor solution drop by drop and stirred in ice-bath for 3 h. Finally, dried $Co_{X\%}@PNC$ nanocomposites were obtained by drying at 80 ℃ in vacuum for 6 h after centrifuging 12000 rpm for 3 minutes and washing with DMF, and the powders were stored in vacuum drier for further use. The accurate mass fraction of Co element in $Co_{0.5\%}@PNC$, $Co_{1\%}@PNC$ and $Co_{2\%}@PNC$ were measured by ICP-MS as 0.015%, 0.047% and 0.053%, respectively.

Table S1 The preparation formulas of PNC nanocomposites with different metal ion doping.

Doping concentration (M)	DMF (μL)	Solution **A** (μL)	Solution **B** (μL)	Solution **C** (μL)
0.5%	940	120	120	60
1%	880	120	120	120
2%	760	120	120	240
3%	640	120	120	360

Characterizations methods. X-ray diffraction (XRD) patterns of PNC and $Co_{X\%}$@PNC catalysts were collected on a Rigaku diffractometer (SmartLab, 9 kW) by Cu Kα radiation (λ=0.15418 nm) with a scan range of 5°- 60° and a step size of 0.01°. UV-vis DRS spectra were measured with test sample preparation by grind catalyst (5 mg) and Barium sulfate (300 mg) thoroughly on Lambda 750 UV/VIS/NIR spectrophotometer (Perkin Elmer). The steady-state photoluminescence spectrum (PL) were collected using a F-7000 fluorescence spectrophotometer (Hitachi) under excitation at 400 nm. The time-resolved fluorescence measurements were detected with a FLS-1000 steady state and transient state fluorescence spectrometer (Edinburgh Instruments Ltd.). Excitation wavelength: 400 nm; detection wavelength: 520 nm. Transmission electron microscopy (TEM) and High-Resolution Transmission Electron Microscopy (HRTEM) images were recorded on Tecnai G2 Spirit Twin and Talos F200 X transmission electron microscope (FEI), respectively. The gaseous reaction products measurements using GC-2014 Gas Chromatograph with GC-TCD and GC-FID instruments (Shimadzu), and the liquid phase products analyzed by ECO IC (Metrohm). The ^{13}C NMR spectra of the liquid product obtained from the reaction with $^{13}CO_2$ and $^{13}CH_3OH$ were collected on AVANCE III HD 400 MHz Digital NMR spectrometer (Bruker).

Photocatalytic Experiments: The CO_2 reduction and CH_3OH oxidation tests were

carried out in a 12 mL sealed Pyrex bottle with 5 mL acetonitrile, 15 μL distilled water and 15 μL methanol, then 4 mg photocatalyst were added into the reaction system above. The reaction system was irradiated under 300 W Xe-lamp with the light intensity of 100 mW cm^{-2} at room temperature for 15 h after degas with CO_2 to remove O_2.

Photoelectrochemical Experiments: All the photoelectrochemical characterizations were performed on the CHI760E electrochemical workstation in a 3-electrode configuration with FTO glass (0.5 m^2) attached with catalyst, Pt sheet and Ag/AgCl (in 3 M KCl) as the working, counter and reference electrodes, respectively. The acetonitrile with 0.1 M tetrabutylammonium hexafluorophosphate ($TBAPF_6$) was filled in the cell as electrolyte. The light source and light density and test conditions were consistent with that in the photocatalytic CO_2 reduction test.

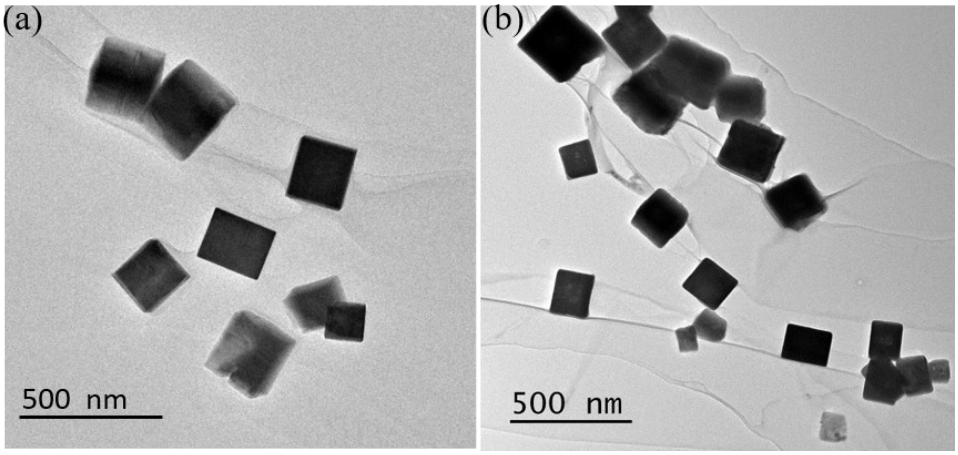

Fig. S1 TEM images of (a) PNC and (b) $Co_{1\%}$@PNC nanocomposites.

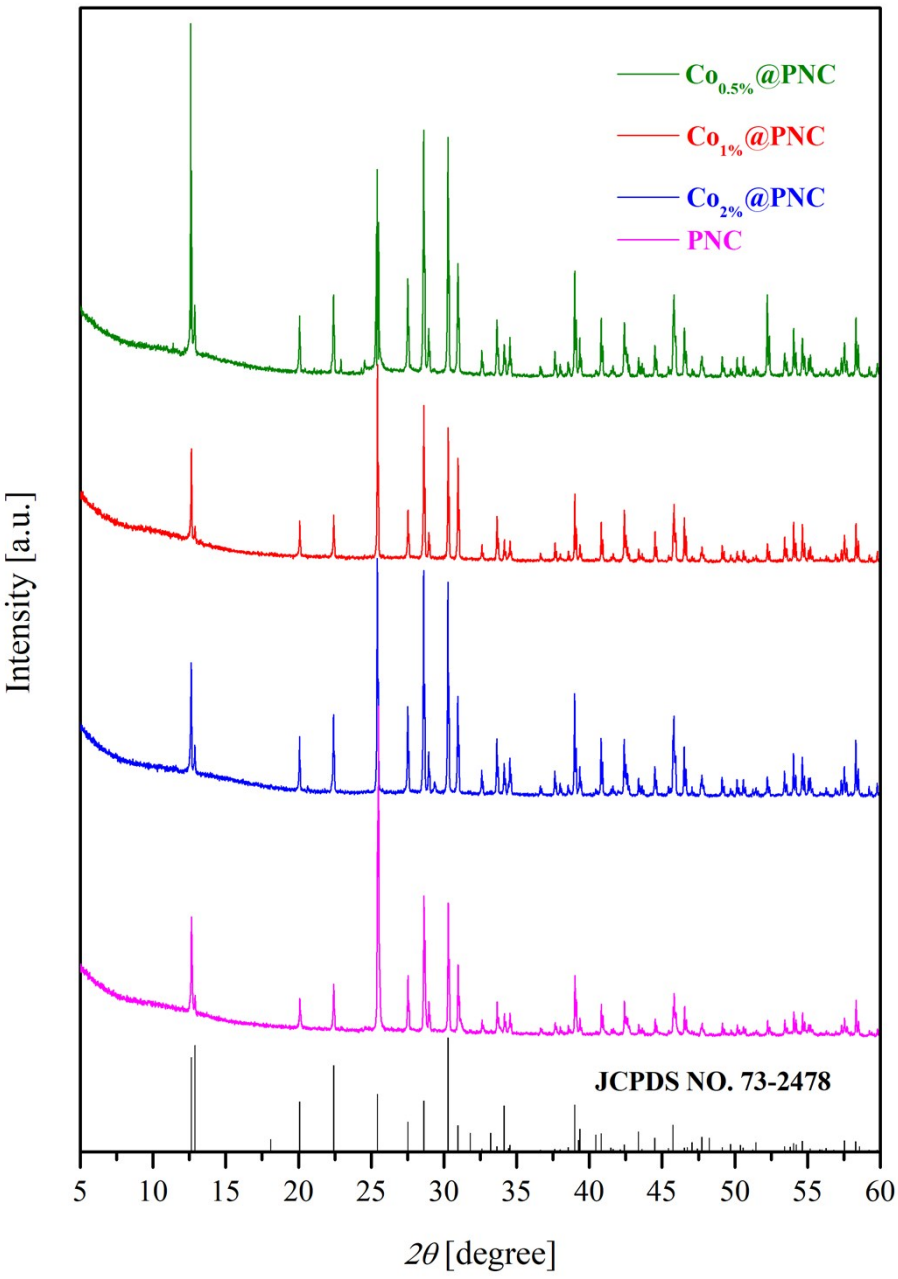

Fig. S2 XRD patterns of the PNC nanocomposites with different Co doping concentrations.

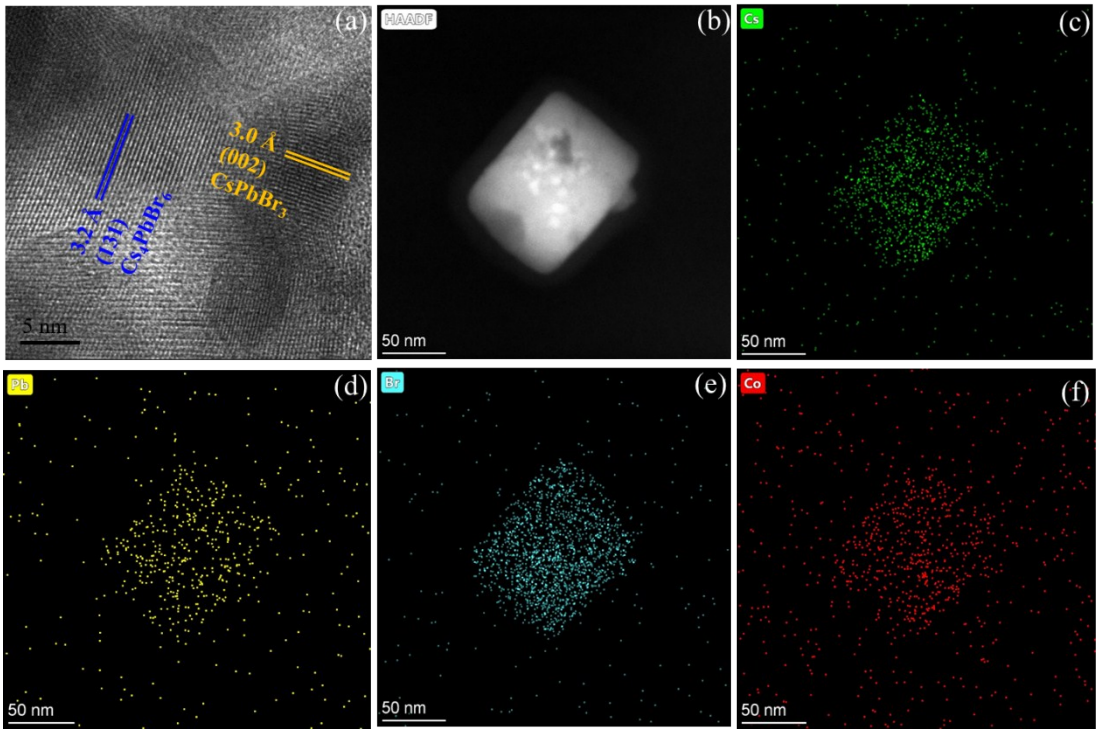

Fig. S3 (a) HRTEM image with lattice spacing of $CsPbBr_3$ (orange) and Cs_4PbBr_6 (blue). (b) TEM image, and (c-f) elemental mappings for $Co_{1\%}@CsPbBr_3/Cs_4PbBr_6$.

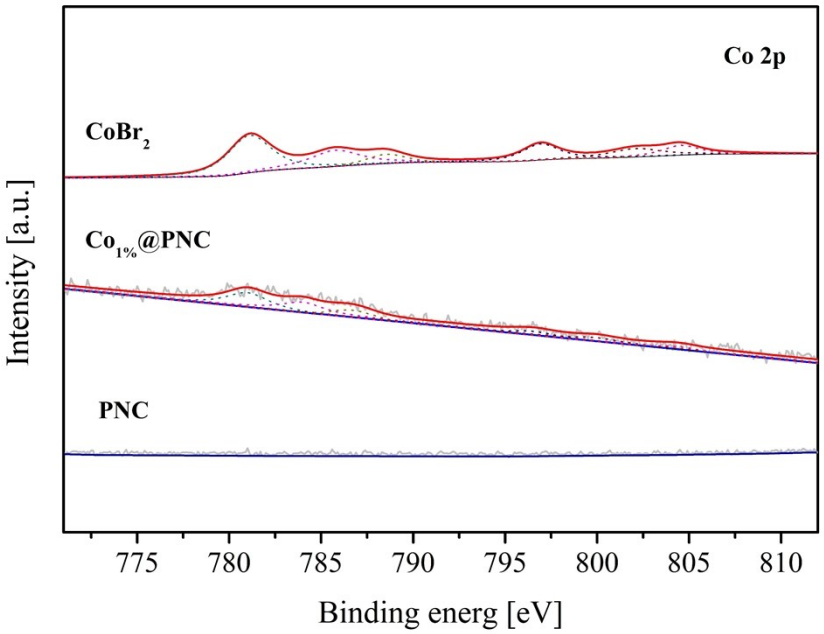

Fig. S4 High resolution XPS plots of Co 2p for $CoBr_2$, $Co_{1\%}$@PNC and PNC samples.

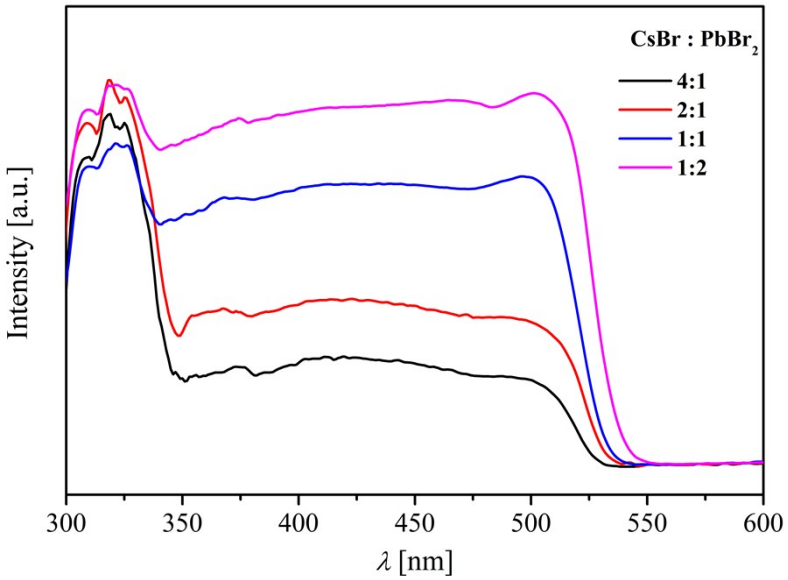

Fig. S5 UV/Vis diffuse reflectance spectra of PNC with different feed ratios of $PbBr_2$ and CsBr.

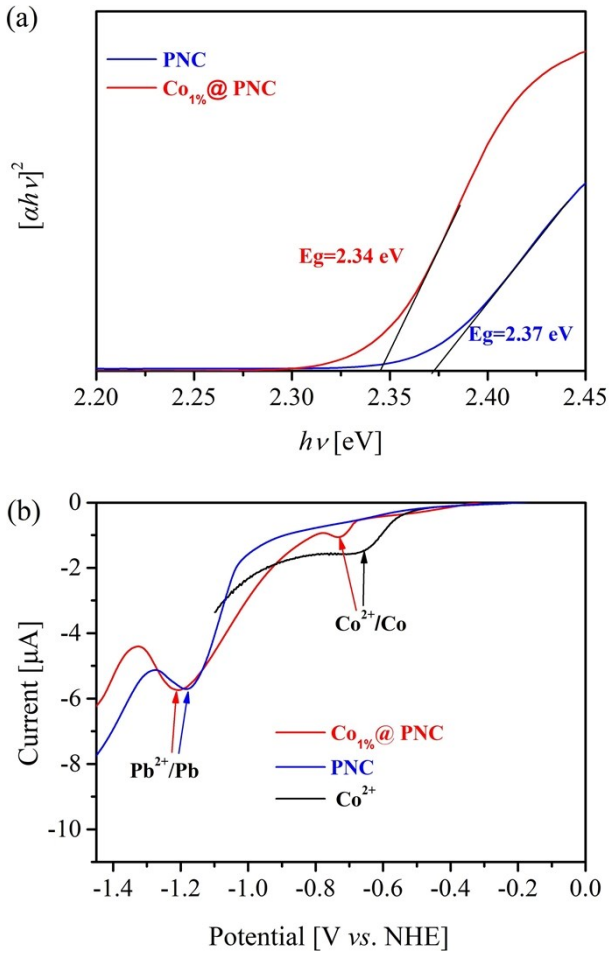

Fig. S6 (a) Tauc plots of PNC and $Co_{1\%}$@PNC. (b) LSV curves of PNC, $Co_{1\%}$@PNC and free Co^{2+} in water under identical conditions.

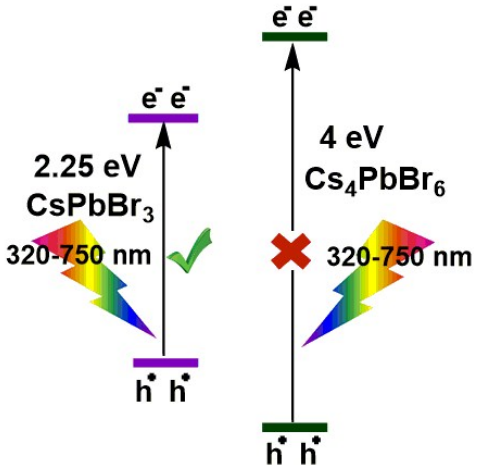

Fig. S7 Schematic illustration of band structures for $CsPbBr_3$ and Cs_4PbBr_6 according to the reported results.[S2]

(a)

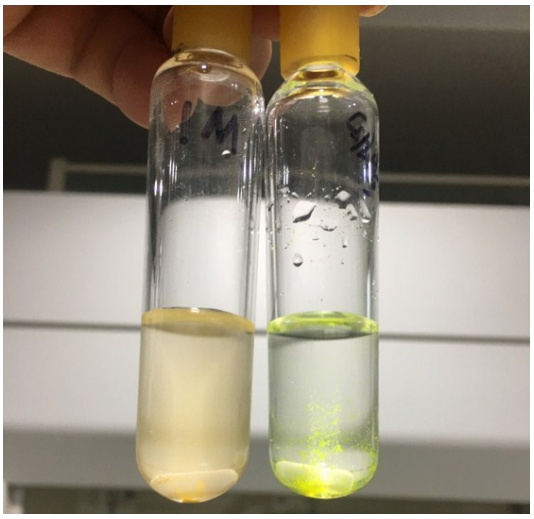

(b)

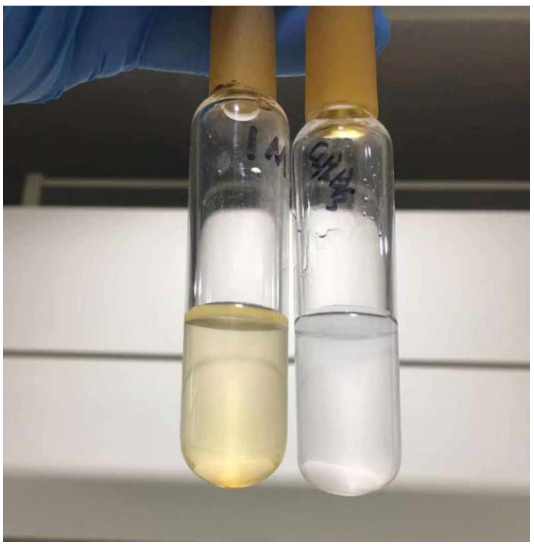

Fig. S8 Comparison before (a) and after (b) the photocatalytic experiments (left: PNC; right: pure $CsPbBr_3$).

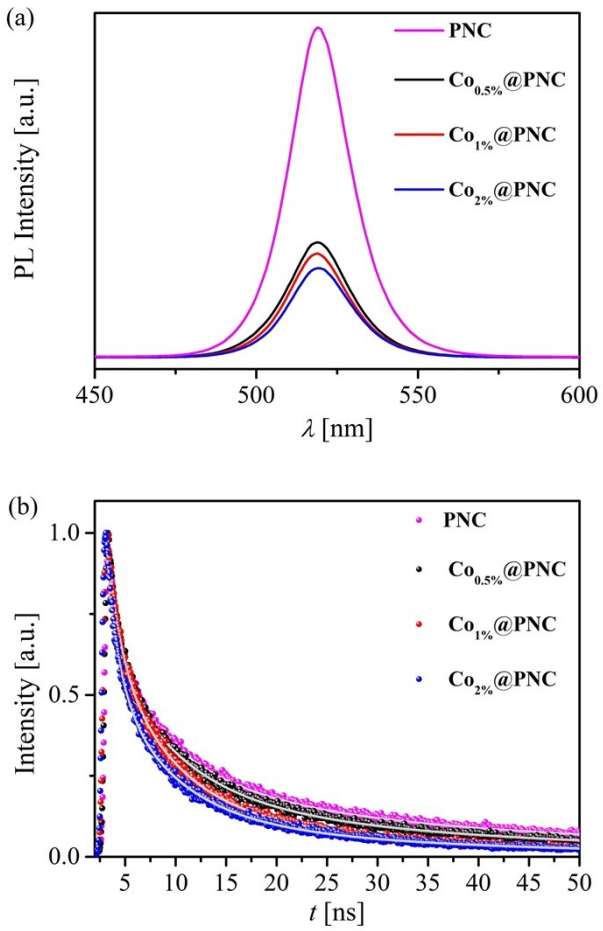

Fig. S9 (a) Photoluminescence spectra and (b) Time-resolved photoluminescence decays of PNC and Co@PNC with various doping concentrations.

Table S2 Multiexponential fit parameters for the decays of photoluminescence lifetime (Fig. S9b). Excitation wavelength: 400 nm; detection wavelength: 520 nm.[a]

sample	τ_1 (ns) (A_1)	τ_1 (ns) (A_1)	τ_1 (ns) (A_1)	τ_{Ave} (ns)
PNC	1.03 (3.46%)	6.50 (26.84%)	30.14 (69.70%)	22.78
$Co_{0.5\%}$@PNC	1.05 (4.43%)	6.57 (33.55%)	27.93 (62.02%)	19.57
$Co_{1\%}$@PNC	1.04 (3.86%)	5.95 (36.84%)	24.92 (55.20%)	16.08
$Co_{2\%}$@PNC	1. 03 (6.81%)	5.80 (38.52%)	22.39 (54.67%)	14.54

[a] $A_1+A_2+A_3=1$; The calculation formula of average lifetime $\tau_{Ave} = \sum\tau_i * A_i$.

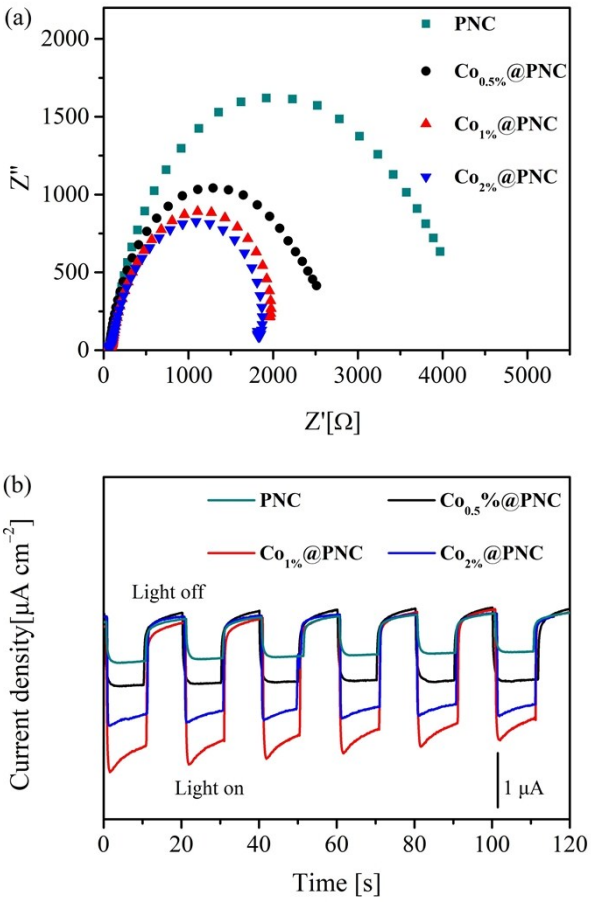

Fig. S10 (a) EIS Nyquist plots of PNC and Co@PNC with various doping concentrations measured under dark. (b) *I-t* curves of PNC and Co@PNC with various doping concentrations plotted at a bias potential of –0.4 V (vs. Ag/AgCl) under light illumination (100 mW cm^{-2}).

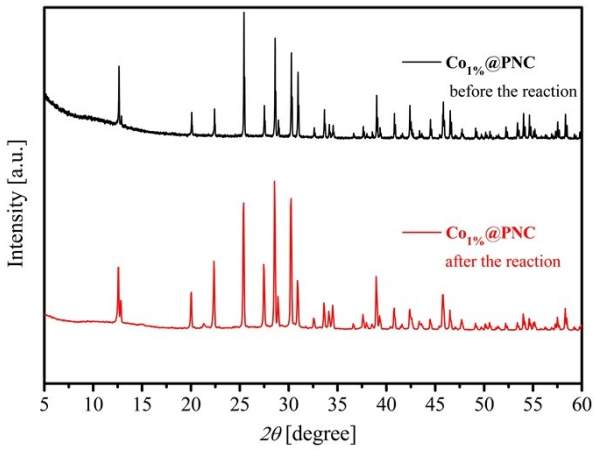

Fig. S11 XRD patterns of $Co_{1\%}$@PNC before (black) and after (red) the photocatalytic reaction.

Table S3 Results of control experiments for the photocatalytic reaction.

Entry	Photocatalyst	Gas Products n_{CO} [μmol]	Liquid Products n_{HCOO^-} [μmol]
1	$Co_{1\%}$@PNC	7.28	3.44
2[a]	0	0	0
3[b]	$Co_{1\%}$@PNC	0	0
4[c]	$Co_{1\%}$@PNC	trace	0.13
5[d]	$Co_{1\%}$@PNC	0.58	0
6[e]	PNC	1.48	---
7[f]	$Co_{1\%}$@PNC	3.02	---
8	Cs_4PbBr_6	0	0
9	$Co_{1\%}$@Cs_4PbBr_6	0	0

Reaction conditions: 4 mg photocatalysts were added into the mixture CO_2-saturated solution of acetonitrile (5 mL), H_2O (15 μL) and methanol (15 μL) under 300 W Xe-lamp irradiation with the light intensity of 100 mW cm^{-2}. Irradiation time: 15 h. [a] Entry 2: without $Co_{1\%}$@PNC photocatalyst. [b] Entry 3: without light. [c] Entry 4: 100% Ar. [d] Entry 5: without methanol. [e]and [f] Entry 6 and 7: methanol replaced with benzyl alcohol.

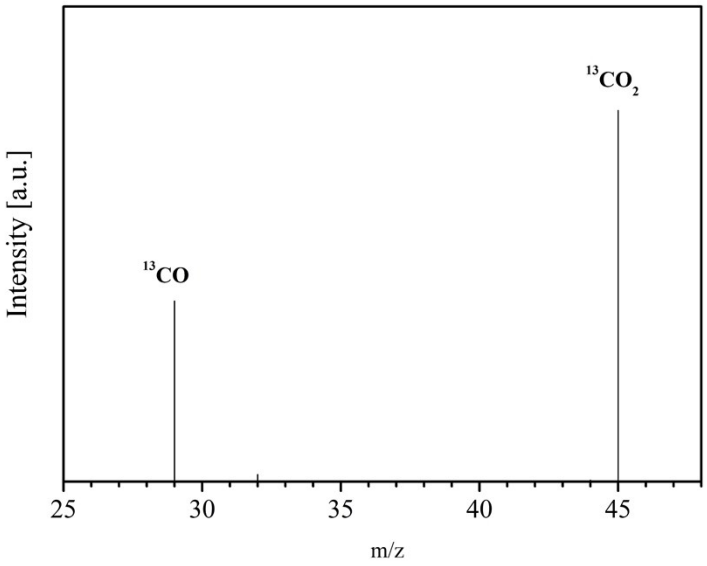

Fig. S12 Gas chromatogram and mass spectra (GC-MS) analysis for solar-driven reduction of $^{13}CO_2$ to ^{13}CO (m/z = 29) with $Co_{1\%}$@PNC as photocatalyst.

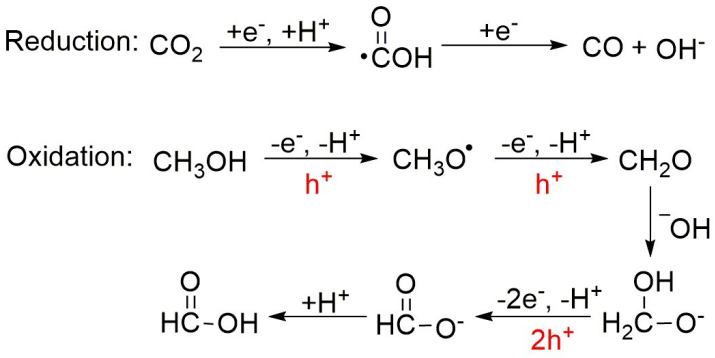

Fig. S13 Proposed mechanistic steps in the reduction of CO_2 and oxidation of CH_3OH.

According to previous literatures,[S3,S4] reasonable reaction pathways for the reduction of CO_2 to CO and the oxidation of CH_3OH to HCOOH have been presented as follows (Fig. S13): For the reduction pathway, initially, photoexcited electron (e^-) can be generated on Co@PNC under light irradiation, the cobalt ions on Co@PNC quickly fixes CO_2 and undergoes a proton-coupled electron transfer (PCET) reduction to generate Co-COOH intermediate. After accepting the second electron, the C-OH bond within Co-COOH is cleaved to give the main reduction product of CO. For the oxidation pathway, firstly, photoexcited hole (h^+) can be generated on Co@PNC under light irradiation. Thus, an electron can be abstracted from the oxygen of hydroxyl group and generate methoxy radical after deprotonation. Because of the strong oxidizability of photoexcited hole on Co@PNC composite, a second subtraction of electron and proton can take place and formaldehyde can be formed. Then a hydroxide formed in the reduction pathway can react with formaldehyde to produce the hemiacetal product, which would continue to be oxidized by the photogenerated hole of Co@PNC composite and form $HCOO^-$. After protonation, the HCOOH can be formed as the main product of methanol oxidation. More detailed mechanistic investigations will be elaborated in future work by in-situ spectroscopic measurements in combination with theoretical simulations.

Reference

S1 J. Li, L. Xu, T. Wang, J. Song, J. Chen, J. Xue, Y. Dong, B. Cai, Q. Shan, B. Han and H. Zeng, *Adv. Mater.*, 2017, **29**, 1603885.

S2 G. Kaur, K. J. Babu, N. Ghorai, T. Goswami, S. Maiti and H. N. Ghosh, *J. Phys. Chem. Lett.*, 2019, **10**, 5302−5311.

S3 A. Call, M. Cibian, K. Yamamoto, T. Nakazono, K. Yamauchi and K. Sakai, *ACS Catal.*, 2019, **9**, 4867−4874.

S4 W. Wu, K. Ding, J. Liu, T Drake, P. Stair and E. Weitz, *J. Phys. Chem. C*, 2017, **121**, 26794−26805.